Contour Estimation on Piecewise Homogeneous Random Fields *

José A. Moinhos Cordeiro
Escola Superior de Tecnologia
Instituto Politécnico de Setúbal, Setúbal, PORTUGAL.
Email:jcordeir@est.ips.pt

José M. Bioucas Dias
Instituto de Telecomunicações
Instituto Superior Técnico, Lisboa, PORTUGAL.
Email: bioucas@lx.it.pt

Key words: Contour Estimation, Bayesian Estimation, Random Fields, Dynamic Programming, Multigrid Methods.

Abstract: This paper addresses contour estimation on images modeled as piecewise homogeneous random fields. It is therefore assumed that images are samples of random fields composed of a set of homogeneous, in a statistical sense, regions; pixels within each region are assumed to be independent samples of a given random variable. Particular attention is given to Gaussian, Rayleigh, and Poisson densities. The model just described accurately fits many class of problems on image modalities such as optical, ultrasound, X-rays, emission tomography, and confocal microscopy, only to name a few. The followed approach is Bayesian: contours are assumed to be *non-causal Markov random fields*. This description is appropriate to include *a priori* information such as continuity, smoothness, elasticity, and rigidity. The selected estimation criterion is the *maximum a posteriori* (MAP). In the present context, MAP estimation, although simpler than others (e.g., minimum mean square error or minimum absolute error), leads to a huge non-linear optimization problem. By using *dynamic programming* associated to a *multigrid* resolution technique, quasi-optimal contour estimates are computed with an acceptable complexity. A set of tests using synthetic and real images illustrates the appropriateness of the proposed methodology.

1 Introduction

Boundary estimation/detection plays a key role in image analysis, pattern recognition, computer vision, computer graphics, and computer-aided animation. Although the approaches to contour estimation are numerous, almost all of them share the same spirit: contours are obtained through the maximization of objective functions composed of a *prior term*, that favors contours with some attributes (e.g., continuity, smoothness, elasticity, and rigidity), and a *data term*, that measures the adjustment to data. As in many other fields, different aspects of contour estimation have been addressed either under the energetic framework or under the Bayesian framework.

*This work was supported by Portuguese PRAXIS XXI program, under project 2/2.1.TIT/1580/95

1.1 Energetic Viewpoint

Under the energetic viewpoint, data and prior terms are interpretable as external energy (e.g., potential) and internal energy (e.g., due to contour *tension* and *rigidity*), respectively. This perspective was introduced in the original work of [Kass 1987], where the concept of *snake* (or active contour, or deformable model) was put out: "A snake is an energy-minimizing spline guided by internal constraint forces and influenced by image forces that pull it towards features such as lines and edges". Since its introduction, the initial concept of snake has been modified and improved in order to adapt it to different images classes and to overcome some of its drawbacks: namely, snake attraction by artifacts, snake degeneration, convergence and stability of the deformation process, myopia (i.e., use of image data only along the contour neighborhood), initialization, and model parameters estimation. References [Cohen 1993], [Zhu 1996], e [Figueiredo 1997] are illustrative examples of approaches to solve common problems with different snake techniques;

1.2 Bayesian Viewpoint

Under the Bayesian viewpoint, the objective function referred to above and its *data* and *prior* terms are interpretable as the *posterior* contour probability, the *likelihood function* associated to the observation mechanism, and the contour *prior* probability, respectively; since the sought contour maximizes the posterior probability it is interpretable as the *maximum a posteriori* (MAP) estimate. In many imaging problems (e.g., medical imaging, synthetic aperture radar, synthetic aperture sonar), the likelihood function can be derived from the knowledge of the generation mechanism, [Figueiredo 1992], [Dias 1996], rather than from other heuristic and common sense arguments. A statistical framework is therefore, in these cases, the correct choice. Relevant advantages of the Bayesian approach are the following:

1. it supplies an adequate framework for the estimation of model parameters, e.g., noise power, parameters distributions, blur coefficients, etc.

2. it is not hampered by *myopia* of snake-type approaches (due to local nature of the *potential* energy), since the likelihood function takes into account all image data.

1.3 Proposed Approach

In this paper we address contour estimation under a Bayesian framework. We assume that images are piecewise homogeneous random fields, and that contours to be estimated are the boundaries of open connected sets. Since the approach is Bayesian the likelihood function and the prior must be specified.

Likelihood Function

The likelihood function is derived from the image observation mechanism. We assume that pixels within each homogeneous region are independent and generated by a selected random variable; both, the considered topologies and the image observation mechanism, are representative of many problems in image analysis, pattern recognition, computer vision, computer graphics and computer aided animation. For example, coherent amplitude images (e.g., ultrasound and synthetic aperture radar and sonar images) are Rayleigh distributed [Wagner 1987], X-ray images are very well approximated with a Gaussian distribution [Makovski 1983], and nuclear and confocal microscopic images are Poisson distributed [Snyder 1991]. We take as hypothesis that the random variables associated with each pixel are independent. It is the so-called *conditional independence property* [Geman 1984]. In an image system, this is a correct assumption if the *resolution volumes* contributing to different pixels are disjoint. This is approximately the case in most acquisition systems, since there is no information gain in acquiring extremely correlated neighboring data. Nevertheless, we will show results in which a wrong

independence assumption still leads to *good* contour estimates.

Prior

Contours are assumed to be samples of *non-causal first order Markov random processes* [Geman 1984]; this class of processes supply a powerful tool for modeling *a priori* knowledge about contours such as continuity.

Estimation algorithm

Contour estimates are obtained according to the MAP criterion. To solve the optimization problem one is led to (joint estimation of contours and of parameters), we adopt the *iterative multigrid dynamic programming* (IMDP) algorithm proposed in [Dias 1996]. According to its name it embodies *iterative*, *dynamic programming*, and *multigrid* concepts.

The methodology herein followed is in vein of works [Dias 1996] and [Dias 1993] on the echographic imaging and [Figueiredo 1992] on X-ray imaging. Main contribution of this work are the following:

1. Generalization of referred methodology to other image modalities;

2. Modification of the estimation algorithm aiming at a robust simultaneous parameter and contour determination;

3. Robustness test against model mismatches.

The paper is organized as follows: Section 2 presents the proposed estimation method; Section 3 describes the implementation algorithm used; Section 4 shows some results of tests made with synthetic and real images; Finally, Section 5 presents the conclusion.

2 Bayesian Approach

Contour estimation is made under the Bayesian framework. Given the vectors $\mathbf{I}$ and $\mathbf{r}$ with, respectively, the image pixel intensities and a contour description, the *a posteriori* probability $\mathbf{P}(\mathbf{r}|\mathbf{I})$ is given by

$$\mathbf{P}\left(\mathbf{r} \mid \mathbf{I}\right) = \frac{\mathbf{P}\left(\mathbf{I} \mid \mathbf{r}\right)\mathbf{P}\left(\mathbf{r}\right)}{\mathbf{P}\left(\mathbf{I}\right)}, \tag{1}$$

where $\mathbf{P}\left(\mathbf{r}\right)$ represents *a priori* contour probability, $\mathbf{P}\left(\mathbf{I} \mid \mathbf{r}\right)$ represents the conditional probability of image given the contour (i.e., the image observation mechanism) and $\mathbf{P}\left(\mathbf{I}\right)$ represents the image probability.

By using the MAP estimation criterion, the estimated contour is then given by [Van Trees 1968]:

$$\begin{aligned} \hat{\mathbf{r}}_{MAP} &= \arg\max_{\mathbf{r}} \left\{\mathbf{P}\left(\mathbf{r} \mid \mathbf{I}\right)\right\} \\ &= \arg\max_{\mathbf{r}} \left\{\mathbf{P}\left(\mathbf{I} \mid \mathbf{r}\right)\mathbf{P}\left(\mathbf{r}\right)\right\}. \end{aligned} \tag{2}$$

So, to obtain the contour estimate $\hat{\mathbf{r}}_{MAP}$ it is necessary to know the image observation mechanism $\mathbf{P}\left(\mathbf{I} \mid \mathbf{r}\right)$ and the *a priori* contour probability $\mathbf{P}\left(\mathbf{r}\right)$. This paper considers three image densities $\mathbf{P}\left(\mathbf{I} \mid \mathbf{r}\right)$: Rayleigh, Gaussian and Poisson. These three densities covers a wide set of images modalities, namely ultrasound, confocal microscopy, X-ray and emission tomography. Examples of the first two modalities are used as test images in this work.

2.1 Image and Contour Representation

Fig. 1 schematizes two contours represented in a polar coordinate system. A two-dimensional representation would be able to describe a wider class of contours. However, we use the polar system since it leads to simpler algorithms and yet it is able to represent contours on a large number of applications such as intravascular ultrasound, echocardiography, ventricular X-ray, cells confocal microscopy, etc.

Image $\mathbf{I}$ is given in a cartesian coordinate system. The image intensity of the pixel at (x, y) is $\mathbf{I}\left(x, y\right)$. To obtain a polar system representation we take M scan lines uniformly spaced, with angle $\theta_i = \frac{2\pi i}{M}$ with $i = 0, \ldots, M-1$. Each scan line vector $\mathbf{I}_i =$

Figure 1: Adopted polar coordinate system and pixels taken from a scan line.

$[x_{i1}, x_{i2}, \ldots, x_{iN_i}]^T$ contains N_i pixels taken along the i*th* scan line as illustrated in Fig 1. The scan line crosses three homogeneous regions. Region (0) and region (1) shares the boundary denoted as $\mathbf{r}^{int}$, while region (1) and (2) shares the boundary denoted as $\mathbf{r}^{ext}$. Using the three region model we have, therefore, two contours to be estimated: these contours are denoted by matrix $\mathbf{r} \equiv \left[\mathbf{r}^{int}, \mathbf{r}^{ext}\right]$, where $\mathbf{r}^{int} \equiv \left[\mathbf{r}_i^{int}\right] = \left[\mathbf{r}_0^{int}, ..., \mathbf{r}_{M-1}^{int}\right]^T$ denotes the distances from the inner contour point to the coordinate center along the i*th* scan line, and $\mathbf{r}^{int} \equiv \left[\mathbf{r}_i^{int}\right] = \left[\mathbf{r}_0^{int}, ..., \mathbf{r}_{M-1}^{int}\right]^T$ denotes the distance from the outer contour.

2.2 Data Generation Probabilistic Models

Pixel intensities, given contour positions and distribution parameters, are assumed independent; it is the so-called *conditionally independence* [Geman 1984]. This hypothesis is correct if resolution volumes that contribute to different pixels are disjoint. As a result we have,

$$\mathbf{P}\left(\mathbf{I} \mid \mathbf{r}\right) = \prod_{i=0}^{M-1} \mathbf{P}\left(\mathbf{I}_i \mid \mathbf{r}_i\right), \tag{3}$$

where $\mathbf{r}_i \equiv \left[\mathbf{r}_i^{int}, \mathbf{r}_i^{ext}\right]$, and

$$\mathbf{P}\left(\mathbf{I}_i \mid \mathbf{r}_i\right) = \prod_{i=1}^{N_i} \mathbf{P}\left(x_{ij} \mid \mathbf{r}_i, \boldsymbol{\theta}_i\right), \tag{4}$$

where $\boldsymbol{\theta}_i \equiv \{\boldsymbol{\theta}_{i1}, \boldsymbol{\theta}_{i2}, \ldots, \boldsymbol{\theta}_{iN_i}\}$ is a vector of parameters usually unknown. Since we are assuming images to be piecewise homogeneous, the vector $\boldsymbol{\theta}_i$ is constant within each region. Therefore,

$$\boldsymbol{\theta}_{ij} = \begin{cases} \boldsymbol{\theta}_i^0 & 1 \le j \le k_i^1 \\ \boldsymbol{\theta}_i^1 & k_i^1 < j \le k_i^2 \\ \boldsymbol{\theta}_i^2 & k_i^2 < j \le N_i \end{cases}, \tag{5}$$

with k_i^1 and k_i^2 being the order number of pixels in the i*th* scan line of the inner and outer contours respectively (see Fig. 1). We now give explicit expressions of the loglikelihood function $\mathbf{L}\left(\mathbf{I}_i \mid \mathbf{r_i}, \theta_\mathbf{i}\right) \equiv \ln \mathbf{P}\left(\mathbf{I}_i \mid \mathbf{r_i}, \theta_\mathbf{i}\right)$ for the Rayleigh, Gaussian (1), Gaussian (2) and Poisson observation models:

Rayleigh Model

Take $\theta_{ij} \equiv \sigma_{ij} \equiv \sqrt{\frac{2}{\pi}} E[x_{ij}]$. We have

$$p\left(x_{ij} \mid \theta_{ij}\right) = \frac{x_{ij}}{\sigma_{ij}^2} \exp\left(-\frac{x_{ij}^2}{2\sigma_{ij}^2}\right), \tag{6}$$

and

$$\begin{aligned} \mathbf{L}(\mathbf{I}_i|\mathbf{r}_i, \boldsymbol{\theta}_i) &= 2k_i^1 \ln\left(\frac{\sigma_i^1}{\sigma_i^0}\right) + 2k_i^2 \ln\left(\frac{\sigma_i^2}{\sigma_i^1}\right) \\ &+ 2N_i \ln\left(\frac{1}{\sigma_i^2}\right) - \frac{1}{2}\left[\sum_{j=1}^{k_i^1}\left(\frac{x_{ij}}{\sigma_i^0}\right)^2\right. \\ &\left. + \sum_{j=k_i^1+1}^{k_i^2}\left(\frac{x_{ij}}{\sigma_i^1}\right)^2 + \sum_{j=k_i^2+1}^{N_i}\left(\frac{x_{ij}}{\sigma_i^2}\right)^2\right] + c \end{aligned} \tag{7}$$

where $\theta_i^0 \equiv \sigma_i^0$, $\theta_i^1 \equiv \sigma_i^1$, and $\theta_i^2 \equiv \sigma_i^2$.

Gaussian Model (1)

Take $\boldsymbol{\theta}_{ij} \equiv (\mu_{ij}, \sigma_{ij})$, where $\mu_{ij} = E[x_{ij}]$, and $\sigma_{ij}^2 = var[x_{ij}]$. We have

$$p\left(x_{ij} \mid \boldsymbol{\theta}_{ij}\right) = \frac{1}{\sqrt{2\pi}\sigma_{ij}} \exp\left[-\frac{1}{2}\left(\frac{x_{ij}-\mu_{ij}}{\sigma_{ij}}\right)^2\right], \tag{8}$$

and

$$\mathbf{L}(\mathbf{I}_i|\mathbf{r}_i,\boldsymbol{\theta}_i) = k_i^1 \ln\left(\frac{\sigma_i^1}{\sigma_i^0}\right) + k_i^2 \ln\left(\frac{\sigma_i^2}{\sigma_i^1}\right) + N_i \ln\left(\frac{1}{\sigma_i^2}\right) - \frac{1}{2}\left[\sum_{j=1}^{k_i^1}\left(\frac{x_{ij}-\mu_i^0}{\sigma_i^0}\right)^2 + \sum_{j=k_i^1+1}^{k_i^2}\left(\frac{x_{ij}-\mu_i^1}{\sigma_i^1}\right)^2 + \sum_{j=k_i^2+1}^{N_i}\left(\frac{x_{ij}-\mu_i^2}{\sigma_i^2}\right)^2\right] + c^{te} \quad (9)$$

where $\boldsymbol{\theta}_i^0 = (\mu_i^0, \sigma_i^0)$, $\boldsymbol{\theta}_i^1 = (\mu_i^1, \sigma_i^1)$, and $\boldsymbol{\theta}_i^2 = (\mu_i^2, \sigma_i^2)$.

Gaussian Model (2)

This model is as in Gaussian (1), with the restriction $\sigma_i^0 = \sigma_i^1 = \sigma_i^2 = \sigma_i$. We have

$$\mathbf{L}(\mathbf{I}_i|\mathbf{r}_i,\boldsymbol{\theta}_i) = -N_i \ln(\sigma_i) - \frac{1}{2\sigma_i^2}\left[\sum_{j=1}^{k_i^1}\left(x_{ij}-\mu_i^0\right)^2 + \sum_{j=k_i^1+1}^{k_i^2}\left(x_{ij}-\mu_i^1\right)^2 + \sum_{j=k_i^2+1}^{N_i}\left(x_{ij}-\mu_i^2\right)^2\right] + c^{te} \quad (10)$$

Poisson Model

Take $\boldsymbol{\theta}_{ij} \equiv \mu_{ij}$, where $\mu_{ij} = E[x_{ij}]$. Then we have

$$p\left(x_{ij} \mid \theta_{ij}\right) = \frac{e^{-\mu_{ij}}\mu_{ij}^{x_{ij}}}{x_{ij}!}, \quad (11)$$

and

$$\mathbf{L}(\mathbf{I}_i|\mathbf{r}_i,\boldsymbol{\theta}_i) = -k_i^1\mu_i^0 - \left(k_i^2 - k_i^1\right)\mu_i^1 - \left(N_i - k_i^2\right)\mu_i^2 + \sum_{j=1}^{k_i^1} x_i \ln\mu_i^0 + \sum_{j=k_i^1+1}^{k_i^2} x_i \ln\mu_i^1 + \sum_{j=k_i^2+1}^{N_i} x_i \ln\mu_i^2 + c^{te} \quad (12)$$

where $\theta_i^0 = \mu_i^0$, $\theta_i^1 = \mu_i^1$ and $\theta_i^2 = \mu_i^2$.

2.3 A priori Probability

In present work *a priori* contour probability is modeled as a first order, non-causal, unidimensional Markov random field [Jain 1989]. This model is adequate to describe previous contour information such as continuity: contour positions over near scan-lines should be also near.

A random vector $\mathbf{r} = [\mathbf{r}_1, \ldots, \mathbf{r}_{N_i}]$ is said to be first order Markovian if

$$P(\mathbf{r}_i|\mathbf{r}_j, j \neq i) = P(\mathbf{r}_i|\mathbf{r}_j, j \in \mathcal{G}_i), \quad (13)$$

for $i \in S = \{0, \ldots, M-1\}$. Sets $\mathcal{G}_i = \{i-1, i+1\}$ and $\mathcal{G} = \{\mathcal{G}_i, i \in S\}$ are termed the *neighborhood* of i and the *neighborhood system*, respectively [Geman 1984], [Besag 1974].

In order to obtain $\mathbf{P}(\mathbf{r})$ we use equivalence between Gibbs distribution and the Markov random fields proved in the theorem of Hammersley-Clifford [Besag 1974]. According this theorem can write

$$\mathbf{P}(\mathbf{r}) = \frac{1}{Z}\exp\left[-\sum_{C\in\mathcal{C}} V_C(\mathbf{r})\right], \quad (14)$$

where Z is a normalization constant and $\mathcal{C}$ the so-called *cliques* set (see [Derin 1986, cap. 11]). In this case $\mathcal{C}$ is given by $\mathcal{C} = \{i\} \cup \{i-1, i\} \cup \{M-1, 0\}$, with $i = 0, \ldots, M-1$. Function $V_C(\mathbf{r}) \equiv V_C(\mathbf{r}_i, i \in C)$, named the clique potential should be chosen in order to represent *a priori* knowledge about contours.

Define $\phi_i(\mathbf{r}) \equiv \sum_{k=1}^{3} \phi_i^k(\mathbf{r})$ with $\phi_i(\mathbf{r})$ given by $\phi_i(\mathbf{r}) \equiv V_{\{i\}}(\mathbf{r}) + V_{\{i-1,i\}}(\mathbf{r})$, where $V_{\{i\}}(\mathbf{r})$ and $V_{\{i-1,i\}}(\mathbf{r})$ represents potentials associated respectively, to cliques $\{i\}$ and $\{i-1, i\}$. We now introduce terms ϕ_i^k with $i = 1, 2, 3$:

(a) - maximum distance limit between contours (k=1),

$$\phi_i^1(r) = \begin{cases} 0 & if R_{\min} < r_i^{ext} - r_i^{int} < R_{\max} \\ \infty & if R_{\min} \geq r_i^{ext} - r_i^{int} \geq R_{\max} \end{cases};$$

(b) - term penalizing the distance between two inner contour points (k=2)

$$\phi_i^2(r) = \alpha_1\left(r_i^{int} - r_{i-1}^{int}\right)^2;$$

(c) - term penalizing the distance between two outer contour points (k=3)

$$\phi_i^3(r) = \alpha_2\left(r_i^{ext} - r_{i-1}^{ext}\right)^2;$$

2.4 Complete model

From the *a priori* probability $\mathbf{P}(\mathbf{r})$ and data generation model $\mathbf{P}(\mathbf{I} \mid \mathbf{r}, \boldsymbol{\theta})$ we have, finally, the *a posteriori* probability

$$\begin{aligned} \mathbf{P}(\mathbf{r} \mid \mathbf{I}, \boldsymbol{\theta}) &\propto \mathbf{P}(\mathbf{I} \mid \mathbf{r}, \boldsymbol{\theta})\, \mathbf{P}(\mathbf{r}) \\ &= \prod_{i=0}^{M-1} P(\mathbf{I}_i \mid \mathbf{r}_i, \boldsymbol{\theta}_i)\, \mathbf{P}(\mathbf{r}) \quad , \end{aligned} \tag{15}$$

In (15) terms not depending on $\mathbf{r}$ were discarded. Taking the natural logarithm from (15) we obtain

$$\begin{aligned} \Psi(\mathbf{r} \mid \mathbf{I}, \boldsymbol{\theta}) &\equiv \ln[\mathbf{P}(\mathbf{r} \mid \mathbf{I}, \boldsymbol{\theta})] \\ &= \sum_{i=0}^{M-1} L(\mathbf{I}_i \mid \mathbf{r}_i, \boldsymbol{\theta_i}) - \sum_{C \in \mathcal{C}} V_C(\mathbf{r}) + c^{te}. \end{aligned} \tag{16}$$

The MAP estimation is then given by

$$\hat{\mathbf{r}}_{MAP} = \arg\max_{\mathbf{r}} \{\Psi(\mathbf{r} \mid \mathbf{I}, \boldsymbol{\theta})\}. \tag{17}$$

Vectors $\boldsymbol{\theta}_i$ are unknown and should be estimated. We use following criterion:

$$\left(\hat{\mathbf{r}}_{MAP}, \widehat{\boldsymbol{\theta}}\right) = \arg\max_{\mathbf{r}, \boldsymbol{\theta}} \{\Psi(\mathbf{r} \mid \mathbf{I}, \boldsymbol{\theta})\}. \tag{18}$$

To obtain solution (18) use the recursive scheme

$$\hat{\mathbf{r}}^{t+1} = \arg\max_{\mathbf{r}} \left\{\Psi\left(\hat{\boldsymbol{r}} \mid \boldsymbol{I}, \hat{\boldsymbol{\theta}}^t\right)\right\} \tag{19}$$

$$\widehat{\boldsymbol{\theta}}^{t+1} = \arg\max_{\boldsymbol{\theta}} \left\{\Psi\left(\hat{\mathbf{r}}^t \mid \mathbf{I}, \boldsymbol{\theta}\right)\right\}. \tag{20}$$

It is straightforward to show that the solutions of (18) are the only stationary points of (19)-(20). Maximization (20) can be computed analytically for each observation model. For example, for the Gaussian (1) model, $\hat{\mu}_i^j$ and $(\hat{\sigma}_i^j)^2$ are the sample mean and the sample covariance inside each region j, respectively. Contrarily to the ease of (20), each step of (19) is very demanding, since Ψ is a nonconvex function of $\mathbf{r}$. A Bellman-Ford type [Bellman 1957] algorithm, introduced in [Dias 1996] therein called IMDP, is proposed to achieve a sub-optimum solution.

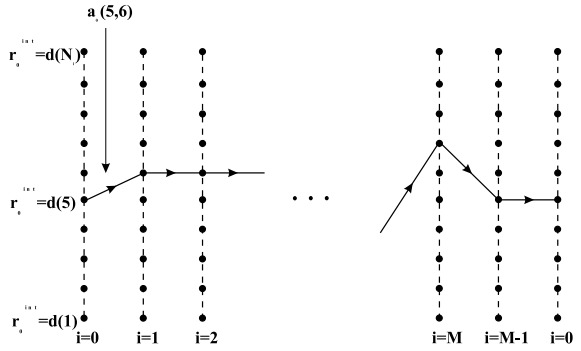

Figure 2: Layered graph associated to the function $\Psi(\mathbf{r}^{int})$

3 Estimation Algorithm

Function Ψ in equation (19) is to be maximized with respect to $\mathbf{r}$. Let $\Psi(\mathbf{r}) = \Psi(\mathbf{r}^{int}, \mathbf{r}^{ext})$ denote Ψ, with $\hat{\boldsymbol{\theta}}^t$ fixed.

Having in mind the definition of vectors $\mathbf{k}_i^1$ and $\mathbf{k}_i^2$, one can write

$$\Psi(\mathbf{r}^{int}, \mathbf{r}^{ext}) = \sum_{i=0}^{M-1} a_i(k_{i-1}^1, k_i^1, k_{i-1}^2, k_i^2), \tag{21}$$

where

$$a_i(k_{i-1}^1, k_i^1, k_{i-1}^2, k_i^2) = L(\mathbf{I}_i | \mathbf{r}_i, \boldsymbol{\theta}_i) - \sum_{k=1}^{3} \phi_i^k(\mathbf{r}). \tag{22}$$

For a while admit also $\mathbf{r}^{ext}$ fixed. This is equivalent to assuming k_i^2 and k_{i-1}^2 fixed. In this case we denote the term $a_i(\cdot)$ in (22) as $a_i(k_{i-1}^1, k_i^1)$, and function $\Psi(\mathbf{r}^{int}, \mathbf{r}^{ext})$ as $\Psi(\mathbf{r}^{int})$.

Maximization of $\Psi(\mathbf{r}^{int})$ is equivalent to finding the high cost path on a directed graph with the set of nodes $\mathcal{N} = \{(i,k) | i = 0, \ldots, M-1,\ k = 1, \ldots, N_i\}$. The cost between node (i,n) and the node $(i-1,m)$, is $a_i(m,n)$; otherwise costs are $-\infty$. Notice that due the cyclic nature of graph, cost a_0 is also defined.

Fig. 2 schematizes the graph and the costs corresponding to the function $\Psi(\mathbf{r}^{int})$. It is a layered graph (each layer corresponds to a

Algorithm A0: Let reals $b_{i,k}$ and integers $n_{i,k}$ be associated to nodes $(i,k) \in \mathcal{N}$. The next recursive scheme provides, the high cost path between node $(0, n_0)$ and node $(0, j)$:
Initialization: $i := 0$; $j := n_0$; $b_{0,k} := -\infty$ (except $b_{0,n_0} := 0$), $k = 0, \cdots, N_0$;
For $i = 1, \cdots, M-1, 0$
For $k = 1, \cdots, N_i$

$$j_{max} := \arg \max_{j=1,\ldots,N_{i-1}} \left(a_i(j,k) + b_{i-1,j}\right)$$
$$b_{i,k} := \left(a_i(j_{max}, k) + b_{i-1,j_{max}}\right)$$
$$n_{i,k} := j_{max}$$

The solution $\mathbf{r}^{int} = [r_0^{int}, \cdots, r_{M-1}^{int}]^T$ is given by:
(1) retrieve solution at node 0 (r_0^{int}):

$$r_0^{int} := d_0(n_0)$$

(2) retrieve solutions at nodes $i = M-1, \cdots, 1$ (r_i^{int}):
For $i = M-1, \cdots, 1$

$$r_i^{int} := d_i(n_{i,r_i^{int}})$$

scan-line), with connections only between pairs of nodes in successive layers. The starting and ending nodes (which are the same given the cyclic topology of the problem) are chosen from scan line $i = 0$.

Suppose, we want to find the high cost path starting and ending at node $(0, n_0)$. This is a dynamic programming problem whose solution is given by Algorithm A0 (Bellman-Ford algorithm [Bellman 1957] tailored to the problem at hand). Therefore, Algorithm A0 provides the contour $\mathbf{r}^{int}$ that maximizes $\Psi(\mathbf{r}^{int})$, constrained to $r_0^{int} = d_0(n_0)$, where $d_i(k)$ is a distance function such that $r_i^{int} = d_i(k_i^1)$ and $r_i^{ext} = d_i(k_i^2)$.

The high cost path, without any constraint, can be achieved by running the algorithm N_0 times, considering that in each run the solution path starts and ends at node $(0, k)$, with $k = 1, \ldots, N_0$. The greatest high cost path is the wanted solution. This approach increases the Bellman-Ford algorithm complexity by a factor of N_0.

Instead of the previous approach, we adopt a suboptimal scheme which is based on the following informal argument: the solution components r_i^{int} corresponding to scan-lines *far from* to scan-line $i = 0$ depend very little on the constraint $r_0^{int} = d_0(n_0)$. Hence, we run Algorithm A0 twice: (1) in the first run the solution is constrained to be $r_0^{int} = d_0(n_0)$, for a given n_0; (2) in the second run the component $r_{\lfloor M/2 \rfloor}^{int}$ (e.g., diagonally opposed to r_0^{int}) is constrained to be that obtained in (1). This scheme takes only 2 runs (instead of N_0) of Algorithm A_0. Although supported a different argument, the strategy just presented was proposed in [Geiger] and therein named *two-loop* method.

For referencing purposes, we present below Algorithm A1 which implements the *two-loop* method. Notation $\mathbf{r}^{int} := \text{Out}\big(\text{A0}[i,a]\big)$ means the solution contour $\mathbf{r}^{int}$ delivered by Algorithm A0 constrained to $r_i^{int} = a$.

Algorithm A1: Implement the *two-loop* scheme.
$\mathbf{r}^{int} := \text{Out}\big(\text{A0}[0, r_0^{int}]\big)$
$\mathbf{r}^{int} := \text{Out}\big(\text{A0}[\lfloor M/2 \rfloor, r_{\lfloor M/2 \rfloor}^{int}]\big)$

Algorithm A1 searches for r_i^{int} over its complete domain. This is not very efficient, thus, one can run algorithm A1 in a *multigrid* type fashion, firstly with a coarse resolution and covering completely the high probability zone, and next refining the estimate by searching in a smaller range, using a thinner resolution.

All the above ideas are implemented simply by constraining the search space to the set of nodes

$$\mathcal{N}[\mathbf{k}^1, m, L] \equiv \{(i,k) | k = k_i^1 + 2^m\, t, \quad t = -L, \ldots, L, \quad i = 0, \ldots, M-1\} \cap \mathcal{N} \quad (23)$$

where $1 \le k_i^1 \le N_i$. Set $\mathcal{N}[\mathbf{k}^1, m, L]$ contains at most $(2L+1)$ nodes corresponding to each scan line, centered at k_i^1 ($r_i^{int} = d_i(k_i^1)$) and 2^m apart. The maximum and the minimum attainable ranges are $\min\left[d_i(k_i^1 + 2^m L, d_i(N_i)\right]$

IMDP algorithm: Assume known $\widehat{\mathbf{r}}_{initial}$, let be given an integer m_0 specifying the coarsest resolution, an integer L specifying the number of searches per layer, and a real $\xi > 0$:
Initialize: $t := 0$, $\mathbf{r} = \widehat{\mathbf{r}}_{initial}$
For $t = 1, 2, \ldots,$

$\widehat{\mathbf{r}} = \mathbf{r}$
Compute $\widehat{\boldsymbol{\theta}}^t$
For $m = m_0, m_0 - 1, \cdots, 0$
$\mathbf{r}^{int} := \mathrm{Out}\big(\mathrm{A1}[\mathbf{r}^{int}, m, L]\big)$
$\mathbf{r}^{ext} := \mathrm{Out}\big(\mathrm{A1}[\mathbf{r}^{ext}, m, L]\big)$
If $\|\mathbf{r} - \widehat{\mathbf{r}}\| > \xi$
continue loop t
Otherwise
$\widehat{\mathbf{r}} = \mathbf{r}$
break loop t

and $\max[1, d_i(k_i^1 - 2^m L)]$, respectively. Concerning Algorithm A1, 2^m denotes the coarseness of search, and $2L+1$ denotes the number of searches per layer.

Define $\mathbf{r}^{int} := \mathrm{Out}(\mathrm{A1}[\mathbf{r}^{int}, m, L])$ as the output $\mathbf{r}^{int}$ of algorithm A1 constrained to the set $\mathcal{N}[\mathbf{k}^1(\mathbf{r}^{int}), m, L]$. All the definitions and concepts supporting algorithm A1 concern the contour $\mathbf{r}^{int}$. They apply equally to contours $\mathbf{r}^{ext}$, replacing index int by index ext, whenever necessary.

Algorithm IMDP, presented below, aims at the efficient determination of estimate $\widehat{\mathbf{r}}$ given by criterion (18), using the iterative scheme (19)-(20).

We could have considered various iterations for each value of m. However, this proved not to be necessary, since for each t, the solution $\mathbf{r}$ provided by the inner **For** loop in the IMDP algorithm is, practically, the wanted one (the maximum of $\Psi(\mathbf{r})$ with respect to $\mathbf{r}$). This fact relies on the relatively high degree of independence (in the statistical sense) between $\mathbf{r}^{int}$ and $\mathbf{r}^{ext}$.

Concerning complexity, the function $\Psi(\mathbf{r}^{int})$ in algorithm A1 has to be computed $N^2 \times M$ times (we are assuming that $N = N_0 = N_1 = , \ldots, = N_{M-1}$). Given a constrained search with $2L+1$ levels, $\Psi(\mathbf{r}^{int})$ has to be computed $(2L+1)^2 \times M$ times. In the present work we adopt $L = 5$. For $N \simeq 150$ this means that the nonconstrained search demands a 185 times larger computational effort compared with the constrained search, what is quite a difference.

4 Results

In this section we present a set of experiments using synthetic and real data. We use $M = 32$ scan lines in all examples. For the images considered, this number represents a good tradeoff between the quality of estimated contours and computational effort (which is proportional to M).

The IMDP algorithm was coded in MATLAB and was parametrized with $m = 3$ and $L = 5$.

The stopping criterion of the IMDP algorithm depends on the parameter ξ. Instead of specifying it, the iteration is stopped when the estimated contours display no more visual changes. In all examples studied, this was accomplished with no more than 4 iterations ($t = 4$).

4.1 Simulated Data

Images shown in Fig. 3, of size 260×185, were generated according to the Rayleigh density. Pixel mean values are $\sigma_i^0 = 10$, $\sigma_i^1 = 30$, and $\sigma_i^2 = 100$. The shape of countours resembles a short axis view of the heart left ventricule.

Fig. 3(b) displays the starting contours obtained by maximizing the log-likelihood of each scan-line $L(\mathbf{I}_i|\mathbf{r}_i, \boldsymbol{\theta}_i)$ with respect to $(\mathbf{r}_i, \boldsymbol{\theta}_i)$. Fig. 3(c) plots the estimated contours over the corresponding image.

Estimates $\widehat{\sigma}_i^0$, $\widehat{\sigma}_i^0$, and $\widehat{\sigma}_i^0$ associated to each scan-line of Fig. 3, computed according to (20), are plotted in Fig. 4.

In the case of the Rayleigh observation model, the performance of the contour estimator depends on the ratios σ_i^1/σ_i^0 and σ_i^2/σ_i^1 (see log-likelihood function (7)). The relative contrast of image in Fig. 3 is $\sigma_i^1/\sigma_i^0 \simeq \sigma_i^2/\sigma_i^1 \simeq 3$,

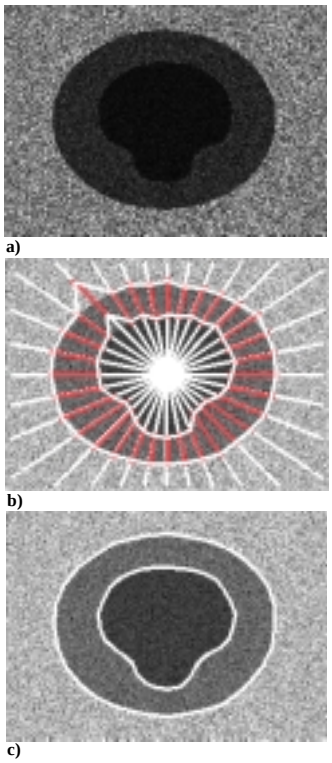

Figure 3: Synthetic Rayleigh image with $\sigma_i^1/\sigma_i^0 = 3$ and $\sigma_i^2/\sigma_i^1 = 3.33$ ($i = 0, \ldots, M-1$): (a) Original image; (b) Starting contours used to initialize IMDP algorithm; (c) Estimated contours.

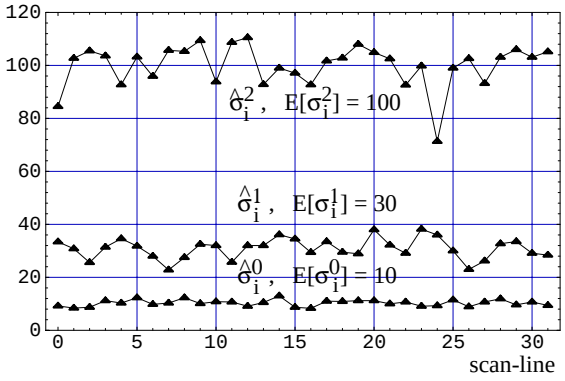

Figure 4: Estimated parameters $\widehat{\sigma}_i^0$, $\widehat{\sigma}_i^1$, and $\widehat{\sigma}_i^2$ associated to each scan-line of Fig. 3(c), for $i = 0, \cdots, M-1$.

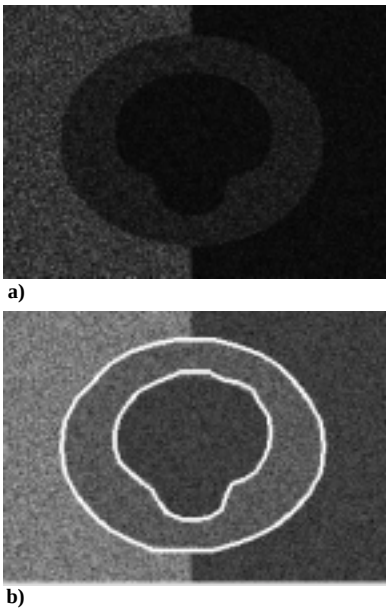

Figure 5: (a) Synthetic Rayleigh image with $\sigma_i^1/\sigma_i^0 = 2$ and $\sigma_i^2/\sigma_i^1 = 2$ on the left hand size and $\sigma_i^2/\sigma_i^1 = 0.5$ on the right hand side; (b) Estimated contours.

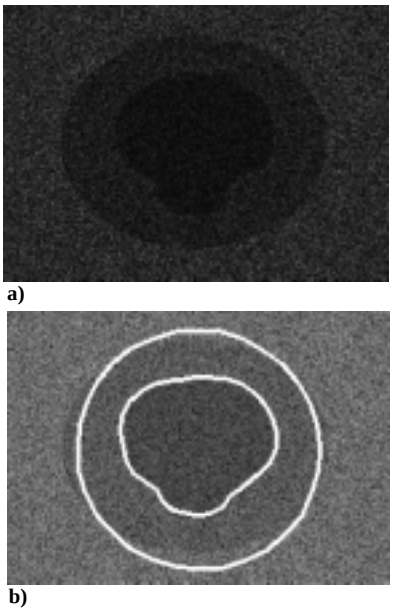

Figure 6: (a) Faint image ($\sigma_i^1/\sigma_i^0 = \sigma_i^2/\sigma_i^1 = 1.5$ for all scan-lines); (b) Estimated contours.

for all scan-lines. This value leads to estimates with good quality.

To have some insight on the trade-off between region contrast and estimation error, Fig. 5(a) displays a Rayleigh image with $\sigma_i^1/\sigma_i^0 = 2$ and $\sigma_i^2/\sigma_i^1 = 2$ for $i = 8, \cdots, 23$ and $\sigma_i^2/\sigma_i^1 = 0.5$ for $i = 24, \cdots, 7$. Compared with the image of Fig. 3(a), there is not only a decrease in the relative contrast from 3 to 2, but also an inversion in the variation of image mean value in the right side of the outer simulated image. This situation occurs frequently with real data. One can say that the estimated contour is a little worse than the one in Fig. 3(c). We have chosen a value of 2 for the relative contrast σ_i^2/σ_i^1, since, with $\alpha_2 = \frac{5\times 10^2}{M^2}$, that value is the limit below which the outer contour becomes biased. Indeed, for $\sigma_i^2/\sigma_i^1 < 2$ the data does not produce enough *strength* to compete with the smoothness term. The net result is a biased outer contour estimate.

Concerning the inner contour, it is possible to have relative contrasts $\sigma_i^1/\sigma_i^0 < 2$ and still have acceptable estimates. Fig. 6 illustrate this situation. The relative contrasts σ_i^1/σ_i^0 and σ_i^2/σ_i^1 were set to 1.5. The outer estimate is biased, mainly near the points were the exterior ellipse shows the greatest curvature. The inner contour estimate is not as good as the one in Fig. 5(b). Roughly, one can say that it is a slightly smoothed version of the estimate plotted in Fig. 5(b). However, it is still good for many quantitative purposes.

4.2 Real Data

Fig. 7(a,b,c) show data obtained by a echocardiographic system, recorded on a video tape, and finally acquired with a video acquisition system. An ultrasound frequency of 2.5 MHz was used.

Figs. 7(b) and 7(c) display the estimated and a hand traced (by an expert) contours, respectively. The Rayleigh observation model was used, since it accurately describes the amplitude in coherent systems such as ultrsound imaging [Makovski 1983]. The agreement between the hand traced coutours and the esti-

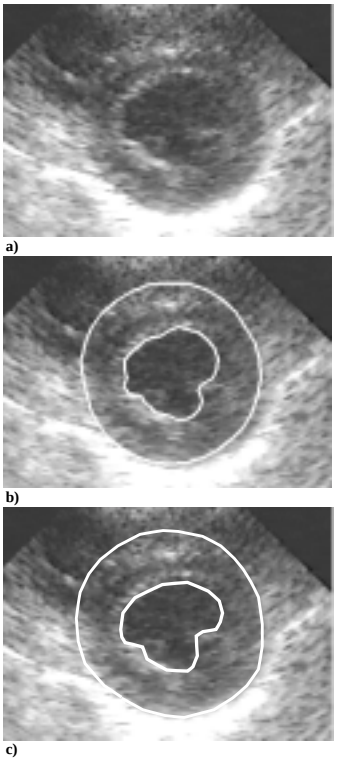

Figure 7: End-systole frame: (a) Original frame; (b) Original frame with automatic contours overlaid; (c) Original frame with hand traced contours overlaid.

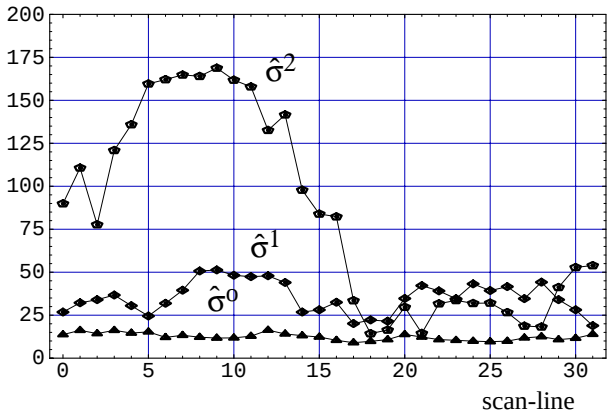

Figure 8: Estimated parameters $\widehat{\sigma}_i$ of image in Fig. **??**(b) for $i = 0, \cdots, M-1$.

mated contour is evident.

Fig. 8 plots the estimated parameters $\widehat{\sigma}_i$ of image in Fig. 7(b) for $i = 0, \cdots, M-1$. We call attention to the almost absence of contrast between scan line 15 and 30. Even though, the contours are well estimated. This is a consequence of the prior information conveyed by the *a priori* Markovian density $P(\mathbf{r})$.

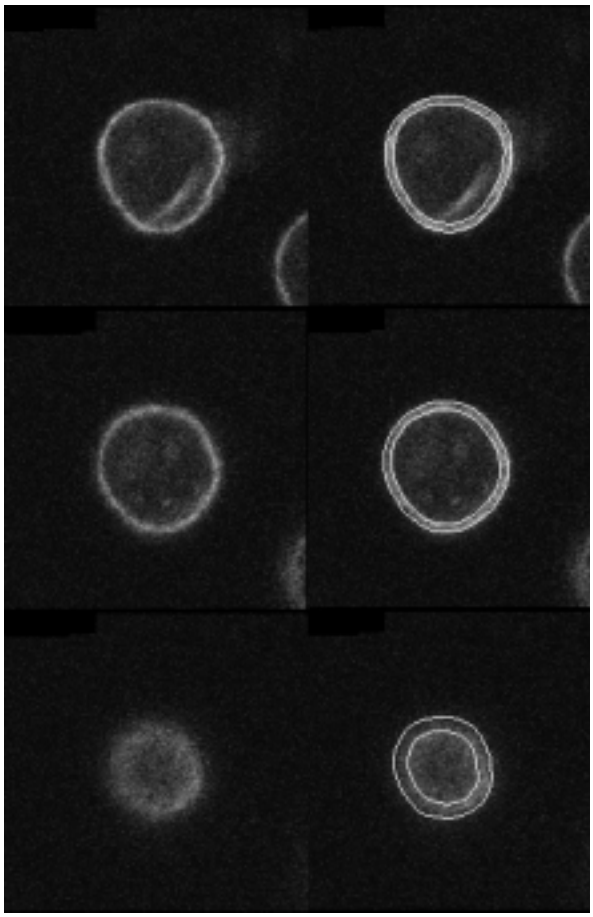

Figure 9: Three confocal microscopy scans of a white blood cell.

Fig. 9, left hand side, shows three confocal microscopy scans of a white blood cell, acquired at different heights. On the right hand side the same images are displayed with contours overlaid. We use the Poisson observation density, given that confocal images are samples of a counting process [Snyder 1991].

The estimated contours are, according to an expert, of good quality. We call attention to the image on the top. It has a mean intensity in inner region that cannot be considered constant, as we assume in our model. Even though, the contours are correctly estimated.

In the course of a research project on the field of genetics, the algorithm herein proposed was applied to more than 20000 images confocal microscopy cell images, many of then containing artifacts, with great success.

5 Conclusion

In this paper a method for contour estimation in piecewise homogeneous images is presented. The problem was formulated under the Bayesian setup. Contours are assumed to be one-dimensional and are modeled as a non-causal first-order Markov random process. The physics of image generation play a key role in building the image generation model; namely, the observed image pixels were modeled as Rayleigh, Gaussian or Poisson distributed random variables with parameters depending on their positions relatively to the contours. The MAP criterion is then applied to derive the contour estimates. To solve the huge optimization problem one is led to, we used an algorithm of the IMDP type introduced in [Dias 1996]. This algorithm embodies dynamic

programming and multigrid aspects.

The method was coded in MATLAB code. In a conventional Personal Computer it takes less than 10 seconds to determine contours from a single image.

References

[Bellman 1957] Bellman, R. 1957 *Dynamic Programming*, Princeton University Press, N.J.

[Besag 1974] Besag, J. 1974, 'Spatial interaction and the statistical analysis of lattice systems', *Journ. Royal Statistical Soc. B,* vol. 36, pp. 192-225.

[Cohen 1993] Cohen, L. & Cohen, I. 1993, 'Finite-element methods for active contour models and baloons for 2D and 3D images', *IEEE Trans. Pattern Anal. Machine Intell.*, vol. 15, pp. 1131-1147.

[Derin 1986] Derin, H. 1986 *Comunications and Networks, A Survey of Recent Advances*, I. Blake and H. Poor Ed., New York.

[Dias 1993] Dias, J. & Leitão, J. 1993, 'Wall Position and Thickness Estimation from Two-dimensional Echocardiograms', *in IEEE Nucl. Sci. Symp., Med. Imag. Conf.*, pp. 1246-1250.

[Dias 1996] Dias, J. & Leitão, J. 1996, 'Wall Position and Thickness Estimation from Sequences of Echocardiographic Images', *IEEE Trans. Med. Imag.*, vol. 15, pp. 25-38.

[Figueiredo 1992] Figueiredo, M. & Leitão, J. 1992, 'Bayesian Estimation of Ventricular Contours in Angiographic Images', *IEEE Trans. Med. Imag.*, vol. 11, pp. 416-429.

[Figueiredo 1997] Figueiredo, M. & Leito, J. & Jain, A. K. 1997, 'Adaptive b-splines and boundary estimation', *in Proc of the IEEE Comp. Soc. Conf. on Com. Vision and Patt. Rec. - CVPR'97*, pp. 724-730.

[Geiger] Geiger, D. & Gupta, A. & Costa, L. & Vlontzos, J. ' Dynamic programming for detecting tracking and matching deformable contours', submitted to *IEEE Trans. Pattern. Anal. Machine Intell.*

[Geman 1984] Geman, S., & Geman, G. 1984, 'Stochastic relaxation, Gibbs distribuition and the Bayesian restoration of images', *IEEE Trans. Pattern Anal. Machine Intell.*, vol. 6, pp. 721-741.

[Jain 1989] Jain, A. 1989, *Fundamentals of Digital Image Processing*, Prentice-Hall, Inc., Englewood Cliffs, N.J.

[Kass 1987] Kass, M. & Witkin, A. & Terzopoulos, D. 1987, 'Snakes: Active contour models', *Intern. Journal of Comp. Vision*, vol. 1, pp. 259-268.

[Makovski 1983] Makovski, A. 1983, *Medical Imaging Systems*, Prentice-Hall, Inc., Englewood Cliffs, N.J.

[Snyder 1991] Snyder, D. L. & Miller, M. I. 1991, *Random Point Processes in Time and Space*, 2nd ed., Springer-Verlag, New York.

[Van Trees 1968] Van Trees, H. 1968, *Detection, Estimation and Modulation Theory*, vol. 1, Jonh Willey, New York.

[Wagner 1987] Wagner, R. F. & Insana, M. F., & Brown, D. G. 1987, 'Statistical properties of radio-frequency and envelope detected signals with applications to medical ultrasound', *J. Opt. Soc. Am.*, vol. 4, pp. 910-922.

[Zhu 1996] Zhu, S. & Yuille, A. 1996, 'Region competition: Unifying snakes, region growing, energy/Bayes/MDL for multiband image segmentation', *IEEE Trans. Pattern Anal. Machine Intell.*, vol. 18, pp. 884-900.